The Institute of Space and Astronautical Science
Report No. 623, October 1987

High Speed and High Angle of Attack Wind Tunnel Test Results of the Winged Space Vehicle C-2

By

Yoshifumi INATANI, Kiyoshi SATO and Keiichi KARASHIMA

(August 20, 1987)

Summary: This paper is concerned with the wind tunnel test results of Winged Space Vehicle executed in 1984 and 1985 at National Aerospace Laboratory (NAL) in Tokyo. The test was conducted and supported by Working Group for Development of a Winged Space Vehicle at the Institute of Space and Astronautical Science (ISAS) to obtain the aerodynamic characteristics of the vehicle recently studied in a preliminary aerodynamic design phase. In the present study, attention has been paid to both longitudinal and lateral/directional stability and controllability at high angles of attack in high speeds that will be encountered by the vehicle at its reentry flight. Test results are summarized in terms of aerodynamic coefficients and their derivatives. Detailed discussions are made to reveal the relations between vehicle configuration and aerodynamic characteristics of the vehicle.

Key words: Winged Space Vehicle, Aerodynamic characteristics, Wind Tunnel Test.

1. INTRODUCTION

Recently, several kinds of development plan of winged space vehicle such as tne US Space Shuttle, for example, or much more advanced concepts have been proposed in the United States, Europe and Japan. Most of these plans and concepts seem to have an intention to accomplish a reentry flight from low earth orbit or an intercontinental flight. At present the US Space Shuttle is an only vehicle which realizes not only a reentry flight but achieves a partly reusable space transportation system as a launch vehicle. However, the vehicles in the next generation are expected to realize a fully reusable or an aircraft-type operation.

In the aerodynamic and flight dynamic design of such vehicles, their configurations must be optimized to have such a sufficient performance so as to accomplish reentry flight from low earth orbit and safety landing to a conventional run way. Therefore, general features of these vehicles may be summarized as follows;

1. reentry flight at high angle of attack that enables to realize moderate deceleration and to avoid excessive aerodynamic heating in hypersonic flight regime,

2. unpowered horizontal landing with minimum lifting surfaces as possible,
3. sufficient stability and controllability throughout the entire ranges of Mach number and angle of attack that these vehicles experience during reentry to final landing.

Furthermore, emphasis is laid on the importance that the vehicles must meet a requirement on weight as a fully reusable rocket vehicle, which is extremely severer than that for conventional airplanes. For instance, the center of gravity position is at about 60% of total length of the vehicle or at more aft-ward position because of the weight-saved tank structure for propellants and rocket engines located at its rear-end *[1]*. Therefore, it must be remarked that the requirements on flight characteristics of the winged space vehicles may be different from those for conventional airplanes *[2, 3]*, and in this sense, flight control strategy must be an unremovable design issue in the design of aerodynamic and flight dynamic performances of the space flight vehicles *[4, 5, 6]*.

In order to satisfy such requirements, investigations must be performed extensively within wide ranges of Mach number and angle of attack. As for the US Space Shuttle, an enormous amount of wind tunnel testing have been conducted *[7]* and those results are partly available *[8, 9]*. In the preliminary design phase of the winged space vehicles, various possibilities in configuration must be studied in order to obtain better understanding of general features of the vehicles' aerodynamic characteristics or the aerodynamically optimum design. It is the purpose of the present study to clarify experimentally the longitudinal and lateral/directional stability and controllability at high angles of attack in high speed flight condition. The relation between the high speed characteristics and low speed performances that is required for a horizontal landing is also investigated.

2. Vehicle Model and Wind Tunnel Test Condition

The model used in the present series of experiment has a configuration of a winged vehicle designed for HIMES (Highly Maneuverable Experimental Space) Vehicle *[10]*, whose concept is proposed as a technology test bed for the development of the future space transportation system. This vehicle is designed as a fully reusable, rocket powered winged vehicle and is expected to satisfy the aerodynamic requirements that the fully reusable reentry vehicle should commonly possess, as mentioned in the previous chapter. The required performances for achieving the reentry flight and the horizontal landing are also very close to those of such future vehicles.

Fig. 1-a shows the basic vehicle configuration proposed for HIMES vehicle at a preliminary stage of the aerodynamic design, which is coded C-2. Dimensions of the vehicle's wind tunnel test model are presented in Table 1. The center of gravity of the vehicle is assumed to be located at 66% of the total length. In the present study, attention is concentrated on the flight dynamic characteristics at high angles of attack. Two types of tail configuration are prepared for the investigation of lateral/directional stability and controllability. Vehicle's control surfaces are conventional elevon, and rudder. Elevon acts as both elevator and aileron. The base line double-tailed

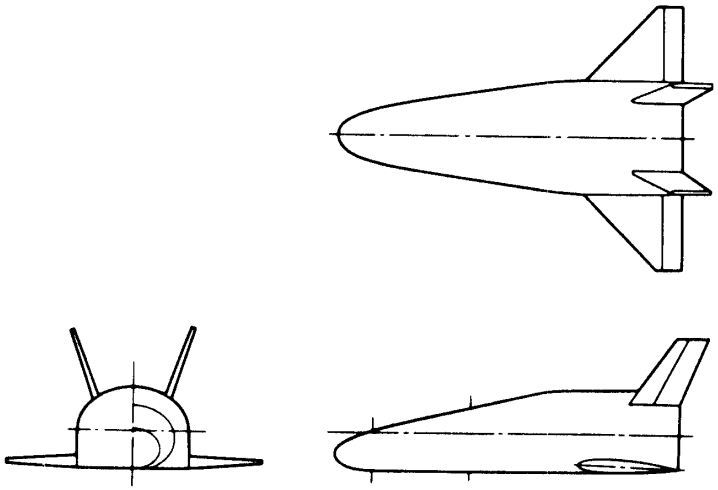

Fig. 1-a. Baseline Vehicle configuration: C–2.

Table 1. Dimensions of vehicle model

Total Length	176.0 mm
Wing Span	133.3 mm
Body Max. Width	57.3 mm
Body Base Area	1870 mm^2
Wing Area (reference area)	6151 mm^2
(exposed)	2407 mm^2
Sweep Back (leading edge)	45.0 deg.
Root Chord	50.67 mm
Tip Chord	12.67 mm
Aspect Ratio (total)	2.89
(exposed)	2.44
Airfoil	NACA-0012
Mean Aerodynamic Chord	54.10 mm
Dihedral	3.0 deg.
Elevon Area	711 mm^2
Chord	9.33 mm
Double Tail Area	960 mm^2
Chord (Root)	24.0 mm
(Tip)	16.0 mm
Rudder Area	384 mm^2
Chord (Root)	9.6 mm
(Tip)	6.4 mm
Single Tail Area	1920 mm^2
Chord (Root)	33.9 mm
(Tip)	22.6 mm
Rudder Area	768 mm^2
Chord (Root)	13.6 mm
(Tip)	9.0 mm
Center of Gravity	116.2 mm (66% from nose)

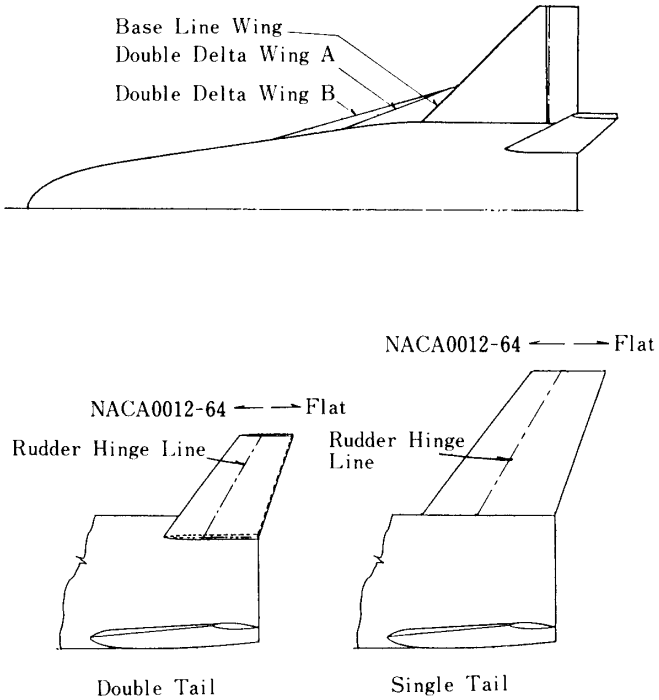

Fig. 1-b. Modification of tail and wing planform.

Table 2. Test condition of wind tunnels

Tunnels	Mach number	Dynamic pressure (kg/cm^2)	Reynolds number*
Transonic	0.7−1.3	0.2 to 0.34	$4.5-5.3\times10^5$
Supersonic	1.6−2.5	0.8	$4.7-5.9\times10^6$
Hypersonic	5.0−7.0	0.35	1.2×10^6

* Reynolds number is based on body total length of vehicle.

configuration has a split type of rudder that is equipped on the outer sides of tail, and conventional rudder is installed for single-tailed configuration. Wing planform is changeable from single delta wing to double delta wing in order to find out the effects on pitching moment and longitudinal stability. These variations are also presented in Fig. 1-b.

Wind tunnels used for the study are transonic (M=0.7 to 1.3), supersonic (M=1.6 and 2.5) and hypersonic (M=5 and 7) tunnels *[11, 12, 13]* of National Aerospace Laboratory (NAL). The test conditions are summarized in Table 2 and the coverage of the test in terms of Mach number and angle of attack is presented in Fig. 2.

In the present study, all of the aerodynamic coefficients and their derivatives are

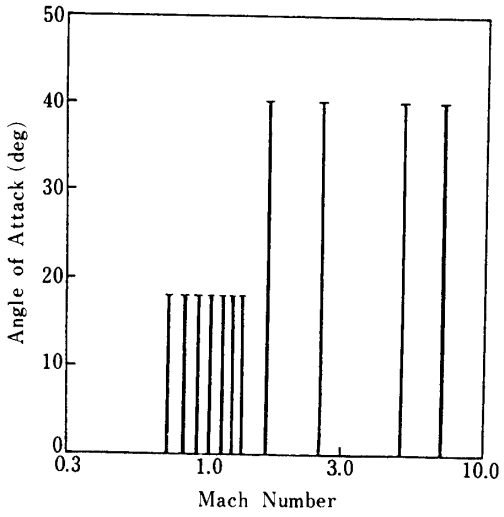

Fig. 2. Coverage of test condition in terms of Mach number and angle of attack.

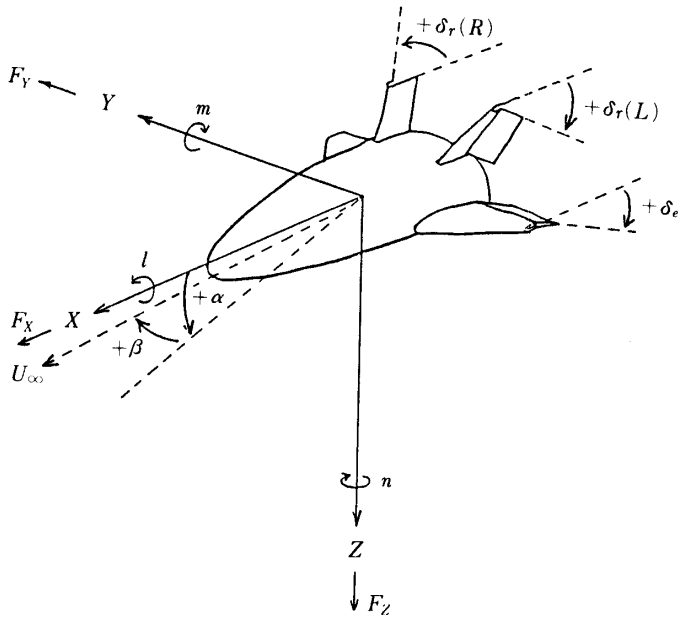

Fig. 3. Definition of coordinate system and control surface deflection.

Table 3. Definition of aerodynamic coefficients and their derivatives

$C_x=F_x/QS$,	$C_y=F_y/QS$,	$C_z=F_z/QS$
$C_l=M_x/QSb$,	$C_m=M_y/QS\bar{c}$,	$C_n=M_z/QSb$
C_L=LIFT/QS,	C_D=DRAG/QS	

$(\ )_\alpha=\partial/\partial\alpha(\ )$	(1/deg)
$(\ )_\beta=\partial/\partial\beta(\ )$	(1/deg)
$(\ )_{\delta e}=\partial/\partial\,\delta e(\ )$	(1/deg)
$(\ )_{\delta a}=\partial/\partial\,\delta a(\ )$	(1/deg)
$(\ )_{\delta r}=\partial/\partial\,\delta r(\ )$	(1/deg)
$(\ )_{\delta SB}=\partial/\partial\,\delta SB(\ )$	(1/deg)

Q	:	dynamic pressure
S	:	reference area
$\bar{c}$	:	mean aerodynamic chord
b	:	wing span
δe	:	elevator deflection angle
δa	:	aileron deflection angle
δr	:	rudder deflection angle $(=(\delta r(L)-\delta r(R))/2)$
δSB	:	speed brake deflection angle $(=\delta r(L)+\delta r(R))/2)$
$\delta r(L)$	:	left side rudder deflection angle
$\delta r(R)$	:	right side rudder deflection angle for double tall configuration

obtained in relation to Mach number and angle of attack. Derivatives related to side slip angle are obtained by use of a sting-support deflected by 5 degrees to the direction of side slip. All the aerodynamic coefficients and their derivatives are expressed according to the conventional aircraft-definitions as shown in Table 3. The deflection angles of control surfaces such as elevon and rudder are defined as shown in Fig. 3. Definition of coordinate system (body fixed axis and wind axis), angle of attack and angle of side slip are also shown in the figure.

3. Test Results

Test results are presented in terms of longitudinal and lateral/directional aerodynamic coefficients. Basic longitudinal aerodynamic coefficients C_L, C_D and C_m are presented in Fig. 4, where results on the elevator deflection is also presented. The derivatives of lift, drag and pitching moment coefficients with respect to the elevator deflection are presented in Fig. 5. Effect of speed brake deflection on those longitudinal coeffIcients at supersonic speed region is presented in Fig. 6. Results of wing planform modification at transonic and supersonic regions are summarized in Fig. 7.

Lateral/directional aerodynamic coefficients such as C_Y, C_l and C_n are presented in terms of derivatives with respect to side slip angle in Fig. 8 and in terms of aileron and rudder deflection angles in Fig. 9 and Fig. 10 respectively. It must be noted that the

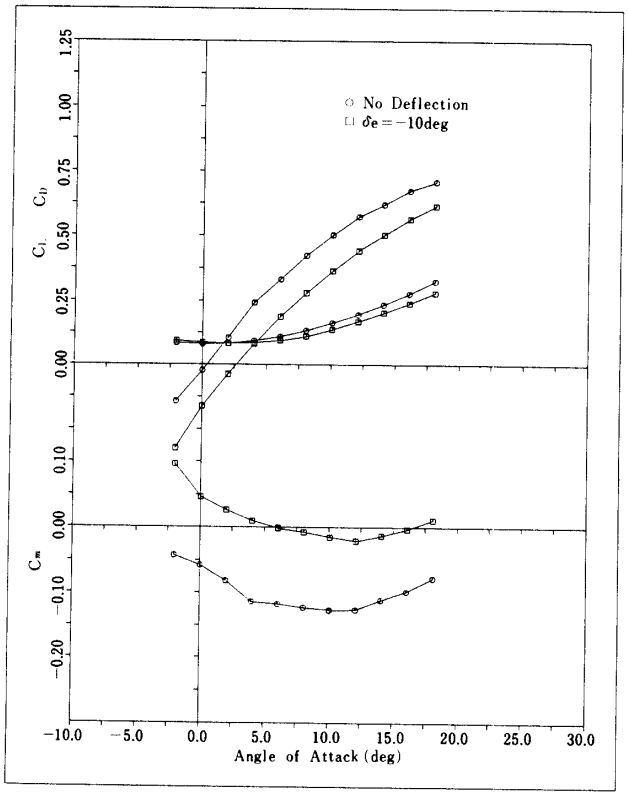

Fig. 4-a. Longitudinal aerodynamic coefficient with elevator deflection (M=0.7).

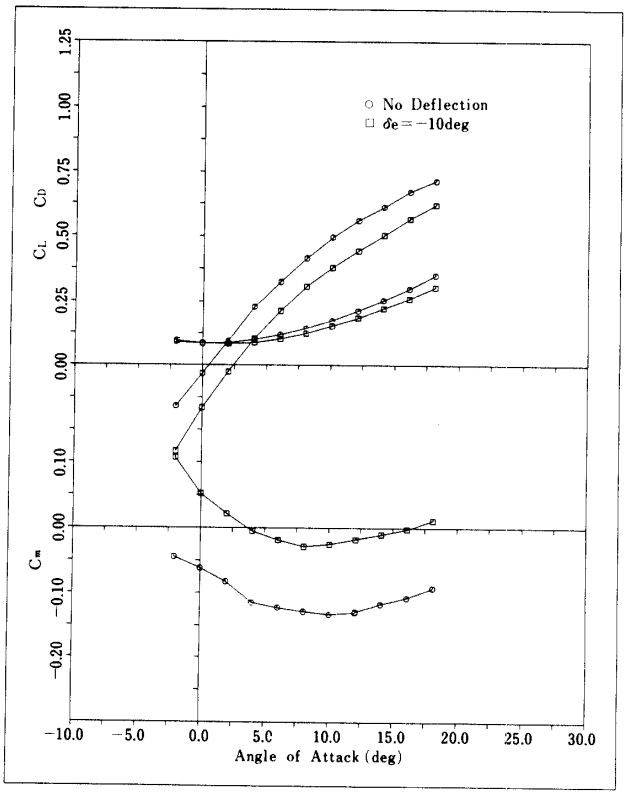

Fig. 4-b. Longitudinal aerodynamic coefficient with elevator deflection (M=0.8).

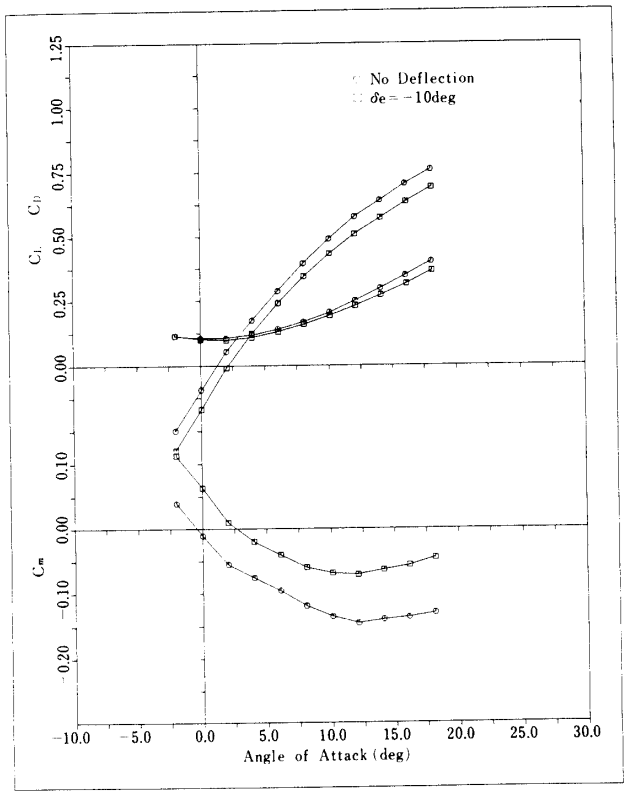

Fig. 4-c. Longitudinal aerodynamic coefficient with elevator deflection (M=0.9).

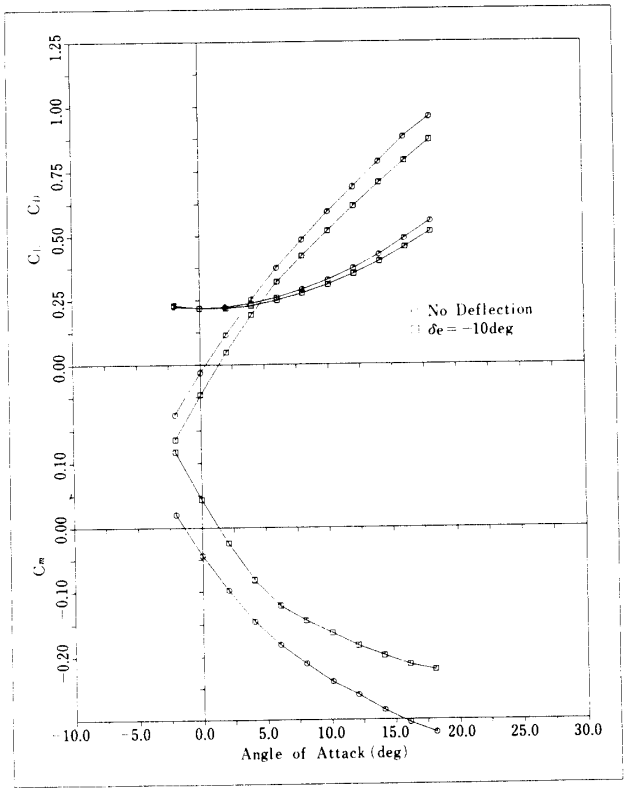

Fig. 4-d. Longitudinal aerodynamic coefficient with elevator deflection (M=1.0).

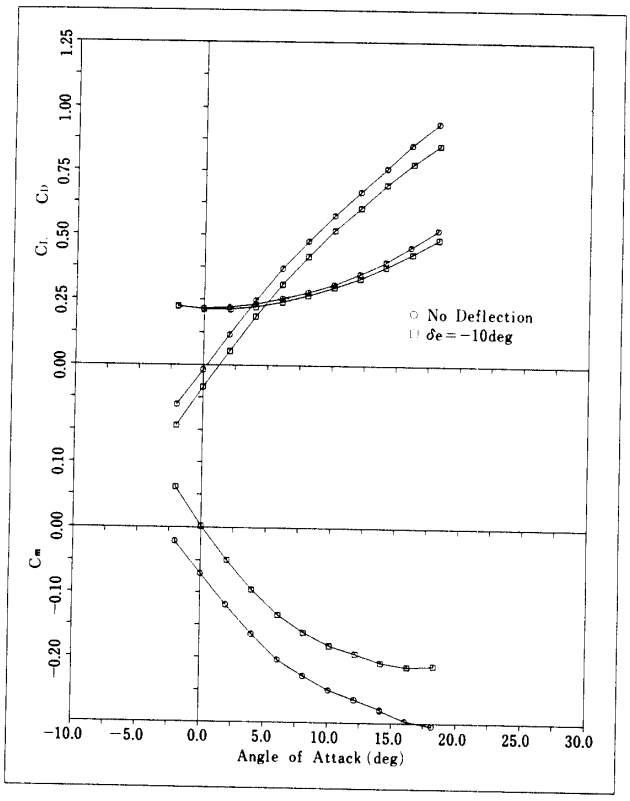

Fig. 4-e. Longitudinal aerodynamic coefficient with elevator deflection (M=1.1).

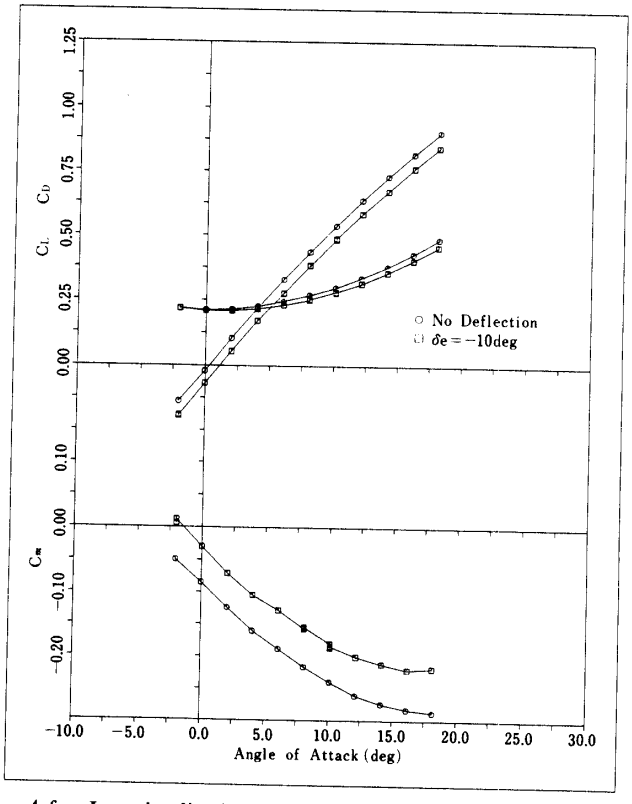

Fig. 4-f. Longitudinal aerodynamic coefficient with elevator deflection (M=1.2).

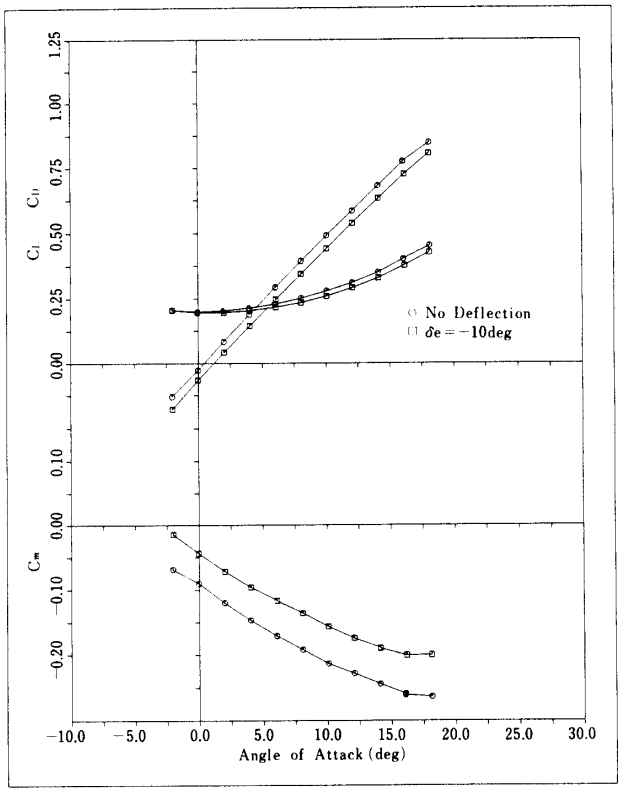

ig. 4-g. Longitudinal aerodynamic coefficient with elevator deflection (M=1.3).

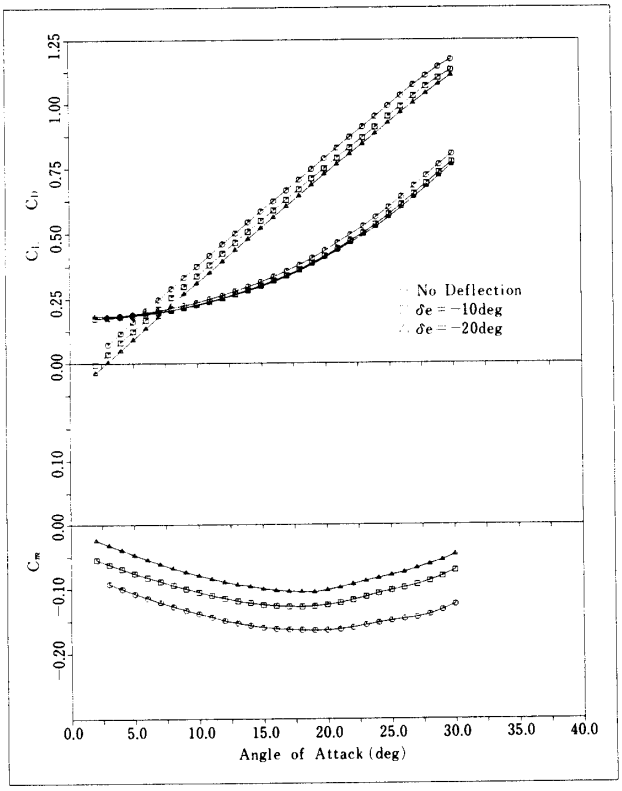

Fig. 4-h. Longitudinal aerodynamic coefficient with elevator deflection (M=1.6).

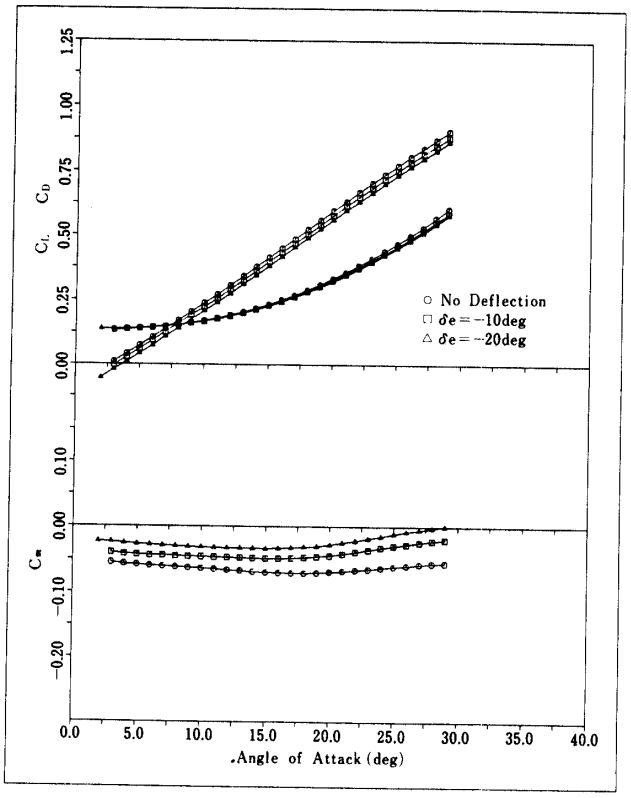

Fig. 4-i. Longitudinal aerodynamic coefficient with elevator deflection (M=2.5).

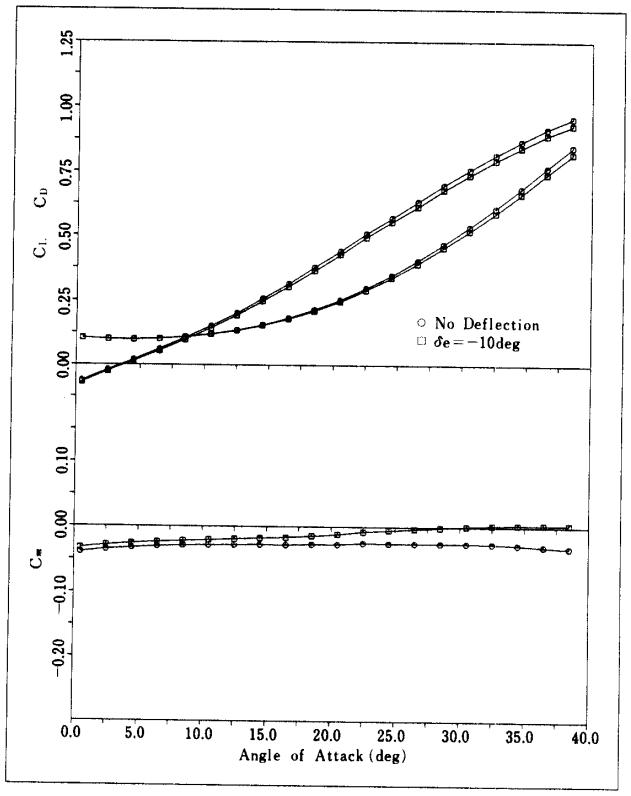

Fig. 4-j. Longitudinal aerodynamic coefficient with elevator deflection (M=5.0).

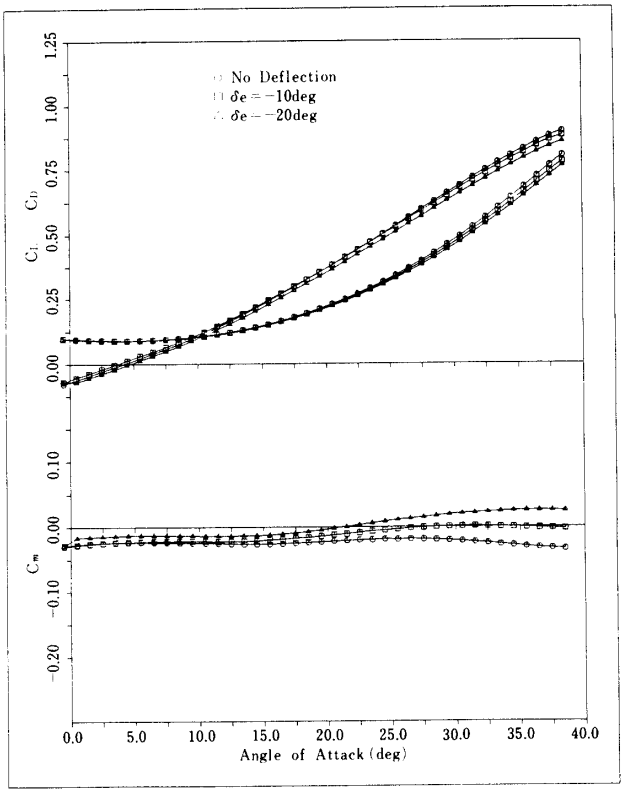

Fig. 4-k. Longitudinal aerodynamic coefficient with elevator deflection (M=7.0).

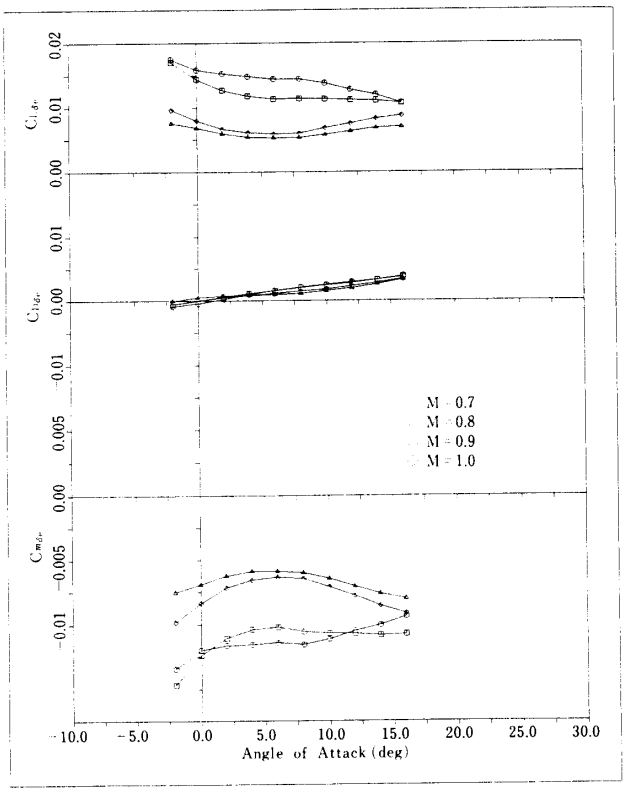

Fig. 5-a. Longitudinal aerodynamic derivatives of elevator M=0.7−1.0 (based on δe=−10 deg data).

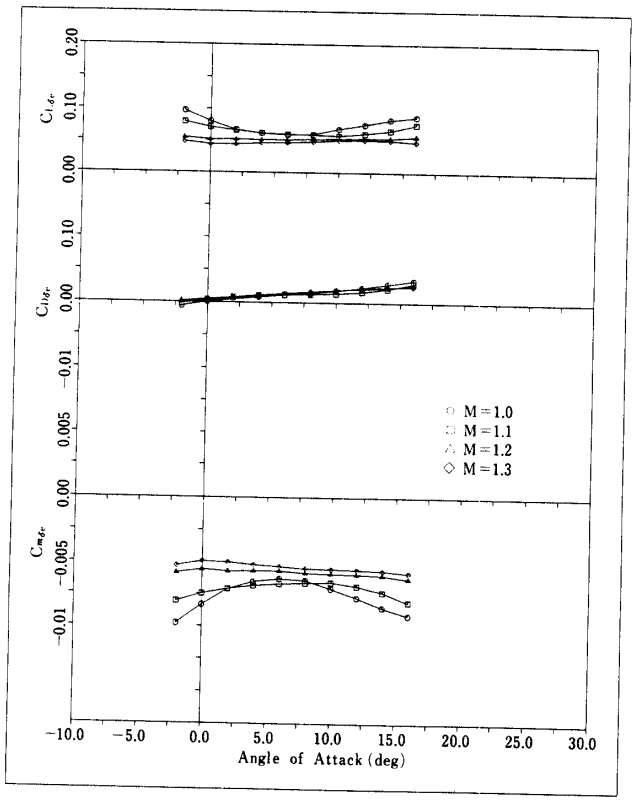

Fig. 5-b. Longitudinal aerodynamic derivatives of elevator M=1.0−1.3 (based on $\delta e=-10$ deg data).

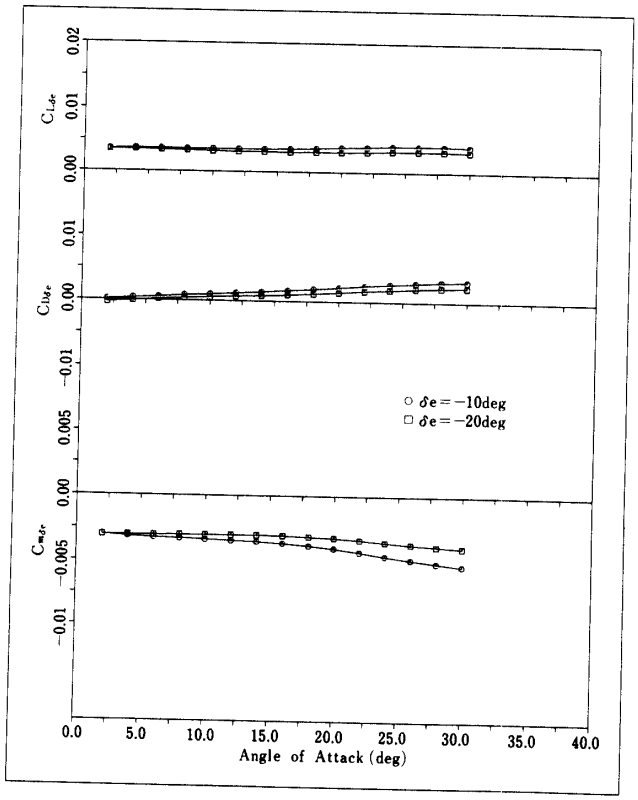

Fig. 5-c. Longitudinal aerodynamic derivatives of elevator M=1.6 (based on $\delta e=-10$ and -20 deg data).

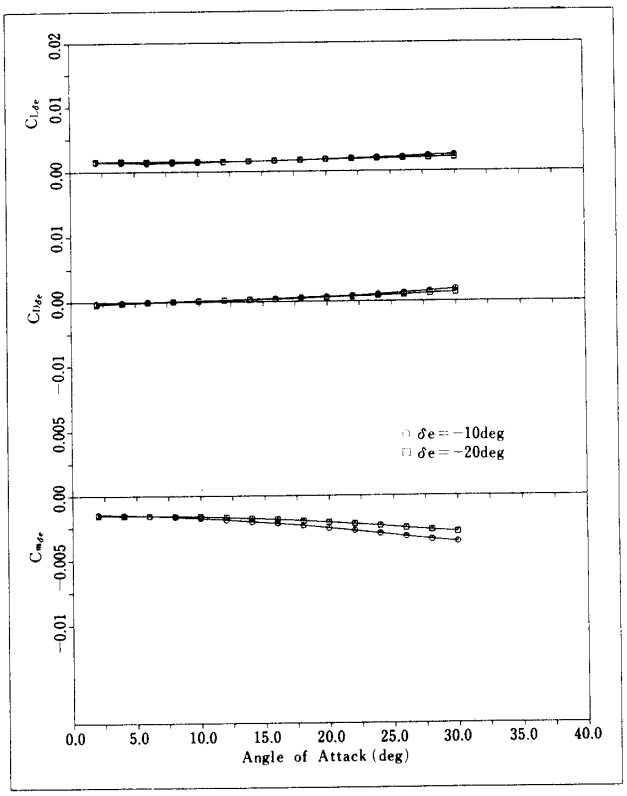

Fig. 5-d. Longitudinal aerodynamic derivatives of elevator M=2.5 (based on $\delta e=-10$ and -20 deg data).

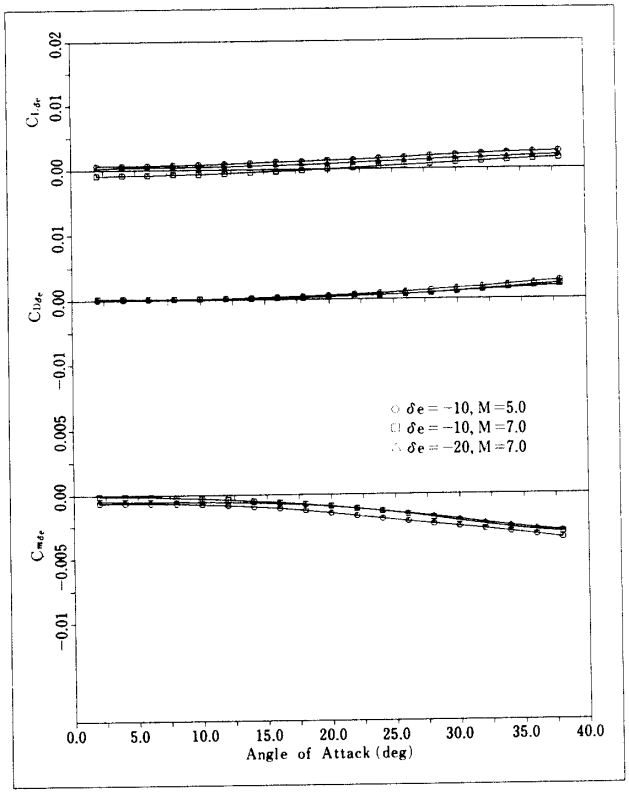

Fig. 5-e. Longitudinal aerodynamic derivatives of elevator M=5.0 ($\delta e=-10$) and M=7 ($\delta e=-10$ and -20 deg data).

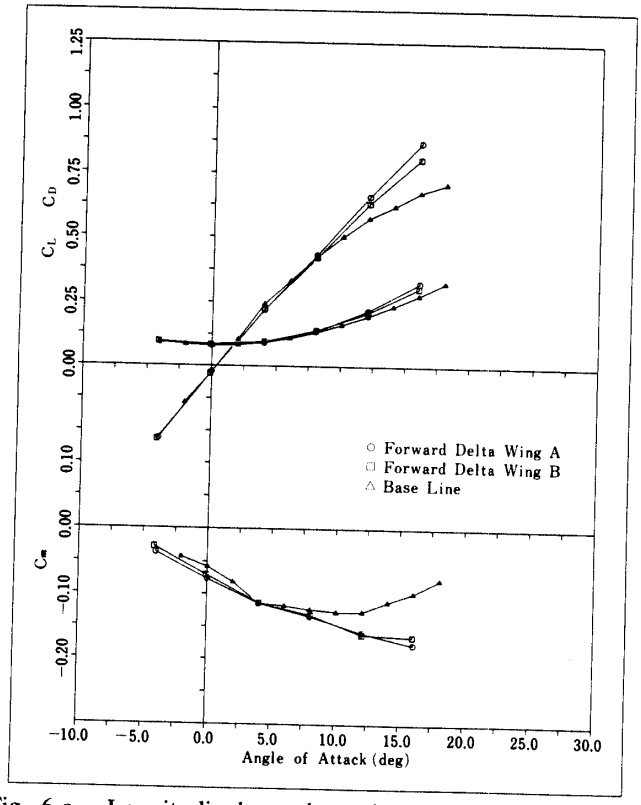

Fig. 6-a. Longitudinal aerodynamic coefficient; forward delta wing on/off (M=0.7).

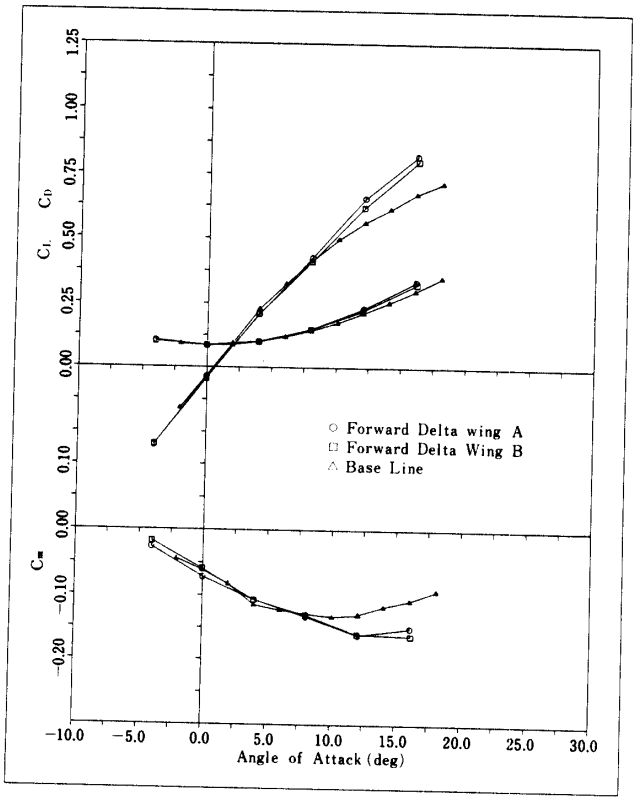

Fig. 6-b. Longitudinal aerodynamic coefficient; forward delta wing on/off (M=0.8).

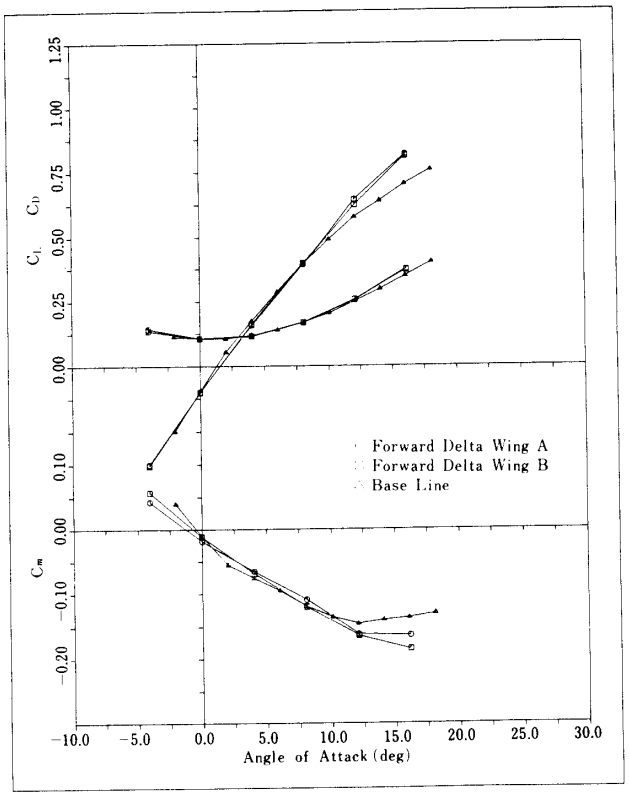

Fig. 6-c. Longitudinal aerodynamic coefficient; forward delta wing on/off (M=0.9).

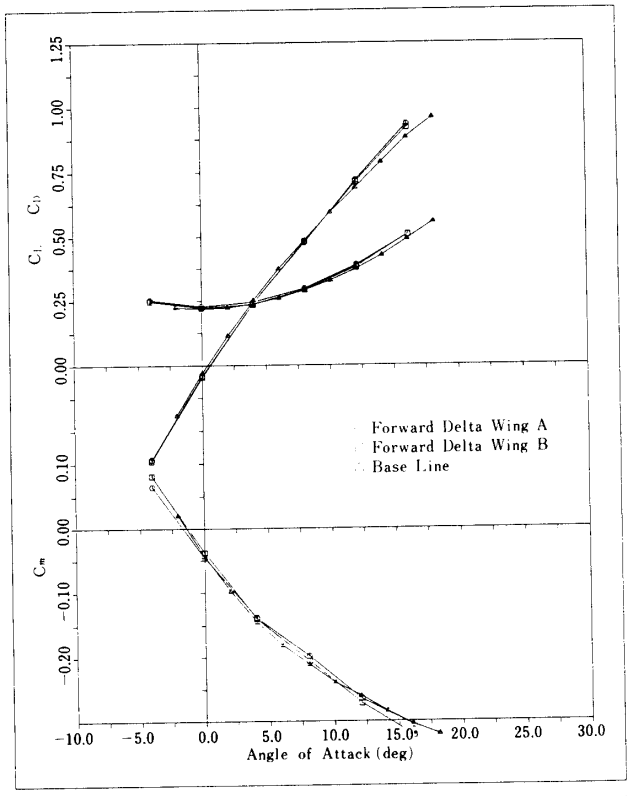

Fig. 6-d. Longitudinal aerodynamic coefficient; forward delta wing on/off (M=1.0).

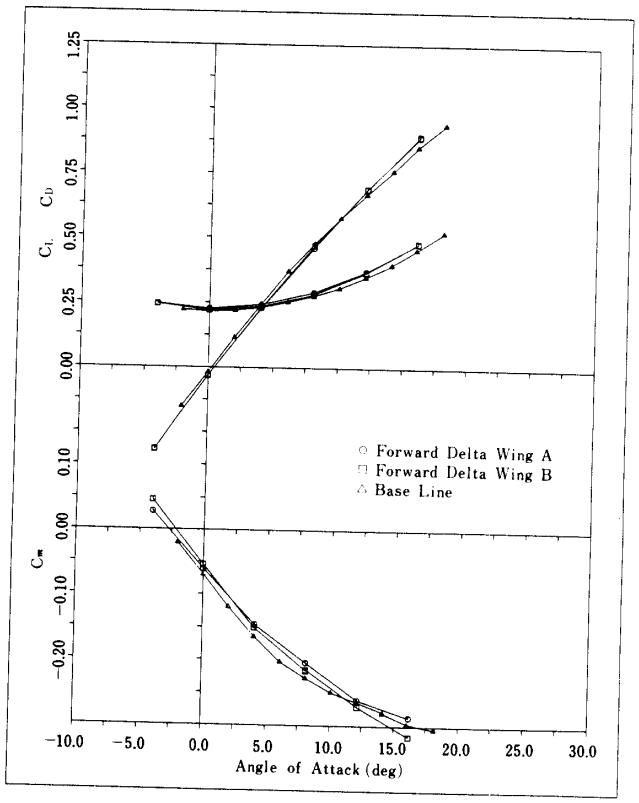

Fig. 6-e. Longitudinal aerodynamic coefficient; forward delta wing on/off (M=1.1).

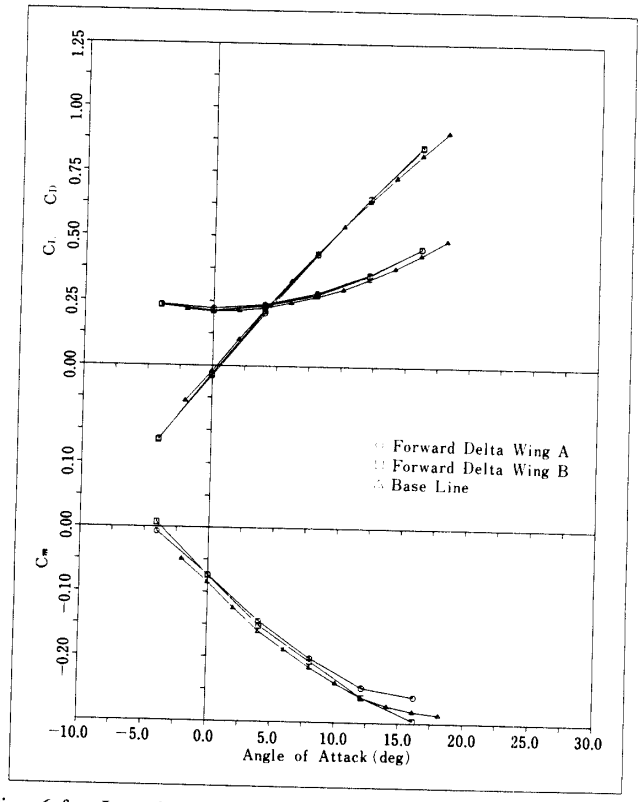

Fig. 6-f. Longitudinal aerodynamic coefficient; forward delta wing on/off (M=1.2).

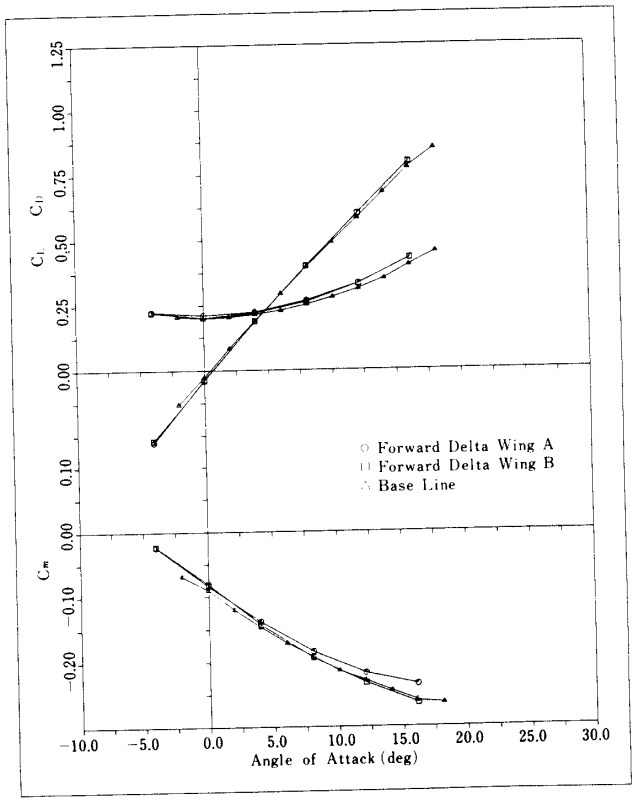

Fig. 6-g. Longitudinal aerodynamic coefficient; forward delta wing on/off (M=1.3).

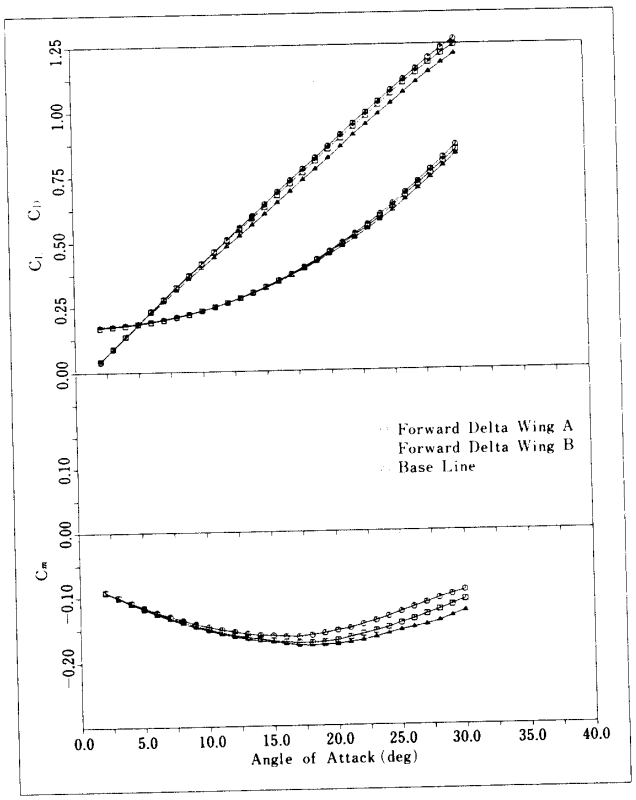

Fig. 6-h. Longitudinal aerodynamic coefficient; forward delta wing on/off (M=1.6).

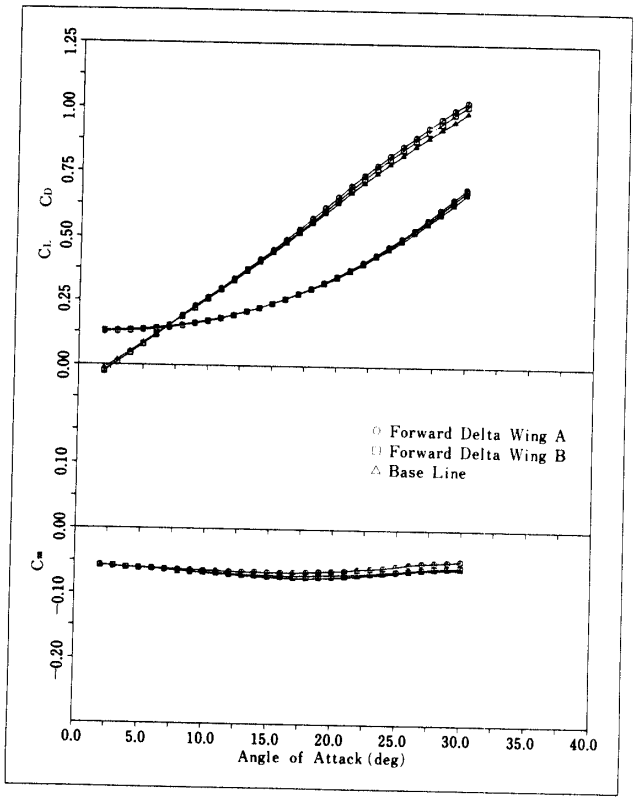

Fig. 6-i. Longitudinal aerodynamic coefficient; forward delta wing on/off (M=2.5).

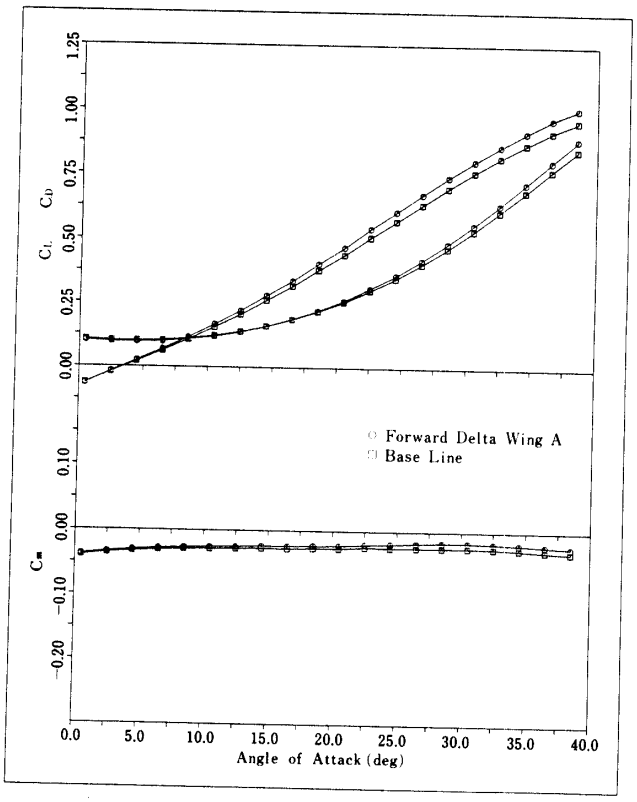

Fig. 6-j. Longitudinal aerodynamic coefficient; forward delta wing on/off (M=5.0).

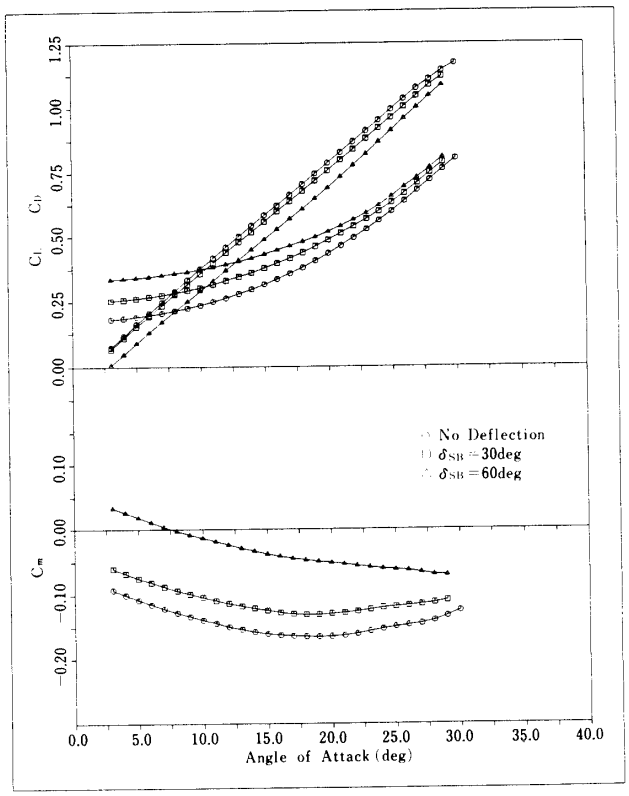

Fig. 7-a. Longitudinal aerodynamic coefficient with speed brake deflection (M=1.6).

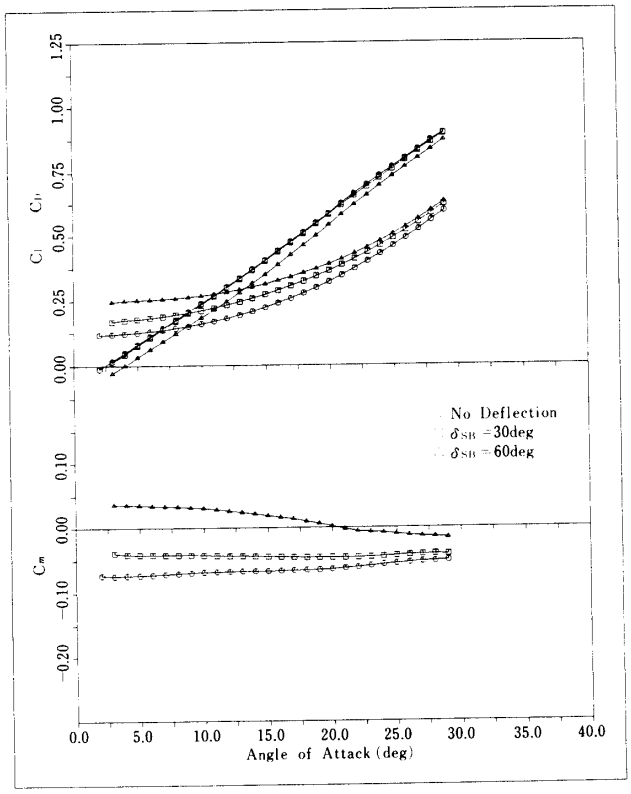

Fig. 7-b. Longitudinal aerodynamic coefficient with speed brake deflection (M=2.5).

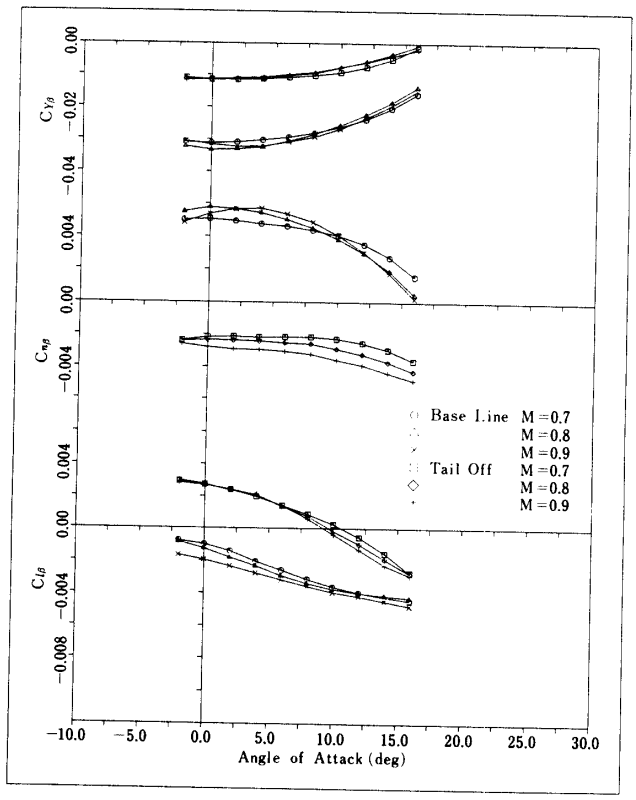

Fig. 8-a. Lateral directional aerodynamic derivatives of side slip angle (M=0.7−0.9).

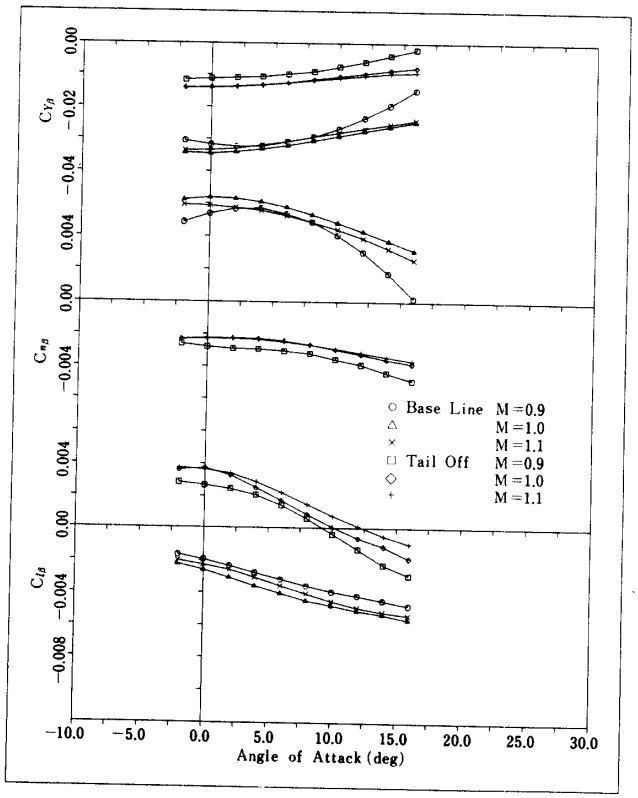

Fig. 8-b. Lateral directional aerodynamic derivatives of side slip angle (M=0.9−1.1).

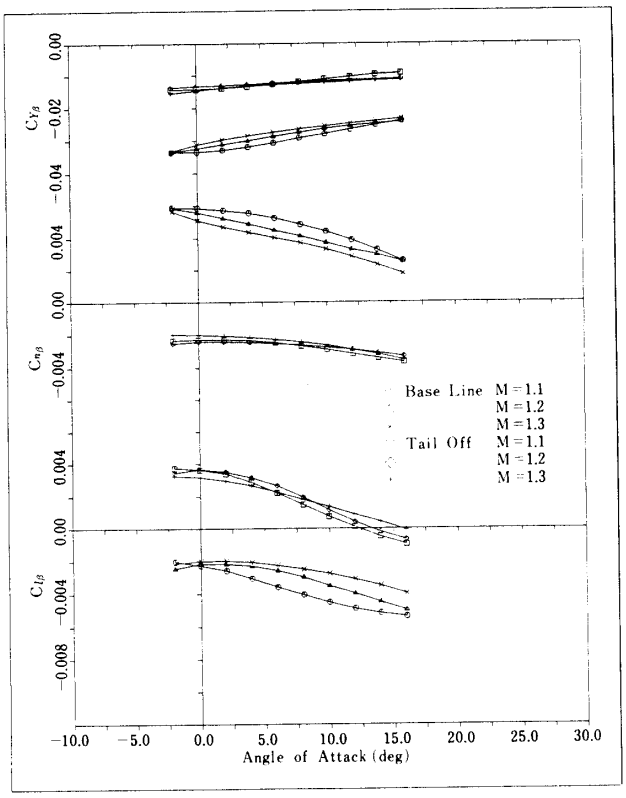

Fig. 8-c. Lateral directional aerodynamic derivatives of side slip angle (M=1.1−1.3).

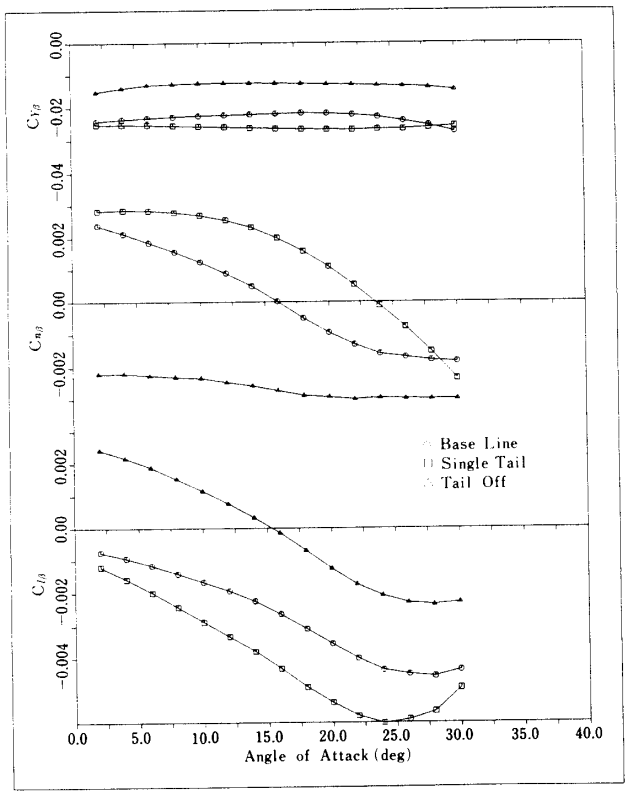

Fig. 8-d. Lateral directional aerodynamic derivatives of side slip angle (M=1.6).

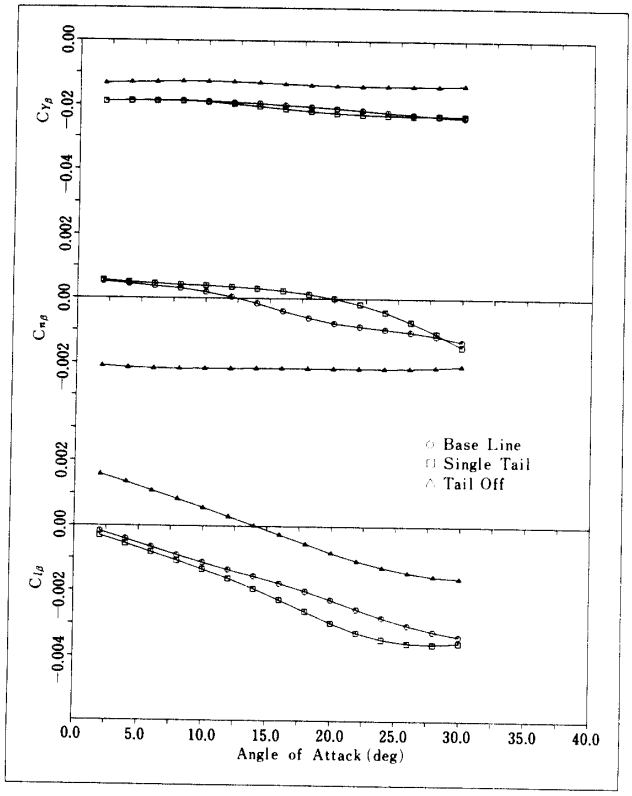

Fig. 8-e. Lateral directional aerodynamic derivatives of side slip angle (M=2.5).

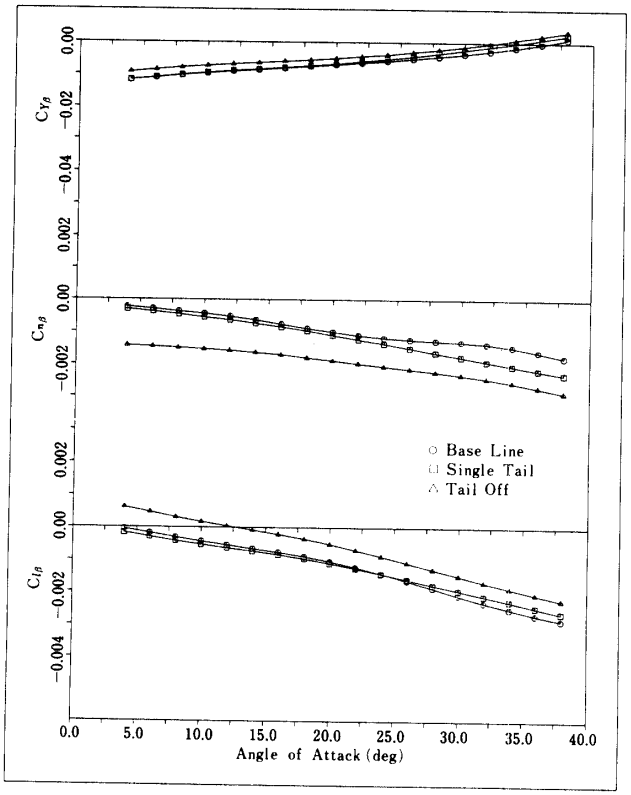

Fig. 8-f. Lateral directional aerodynamic derivatives of side slip angle (M=5.0).

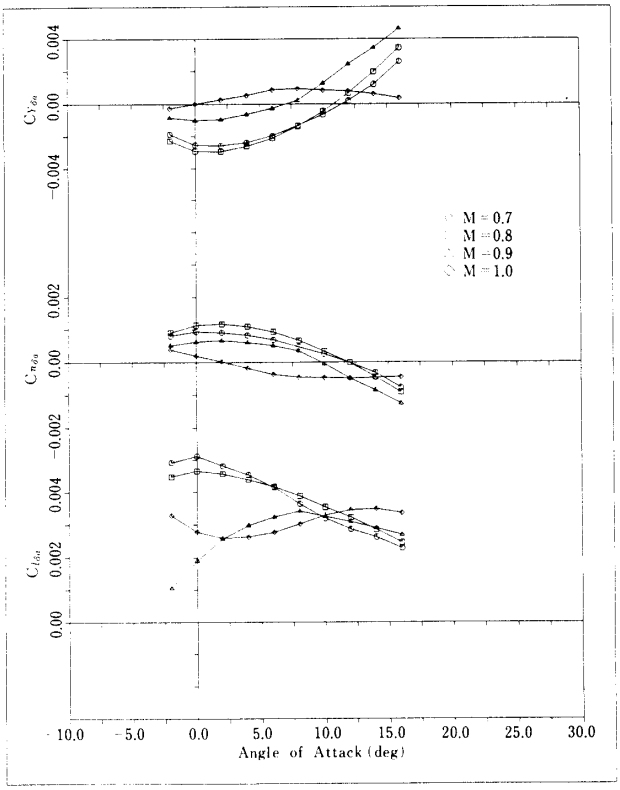

Fig. 9-a. Lateral directional aerodynamic derivatives of aileron deflection (M=0.7−1.0 based on δa=5 deg data).

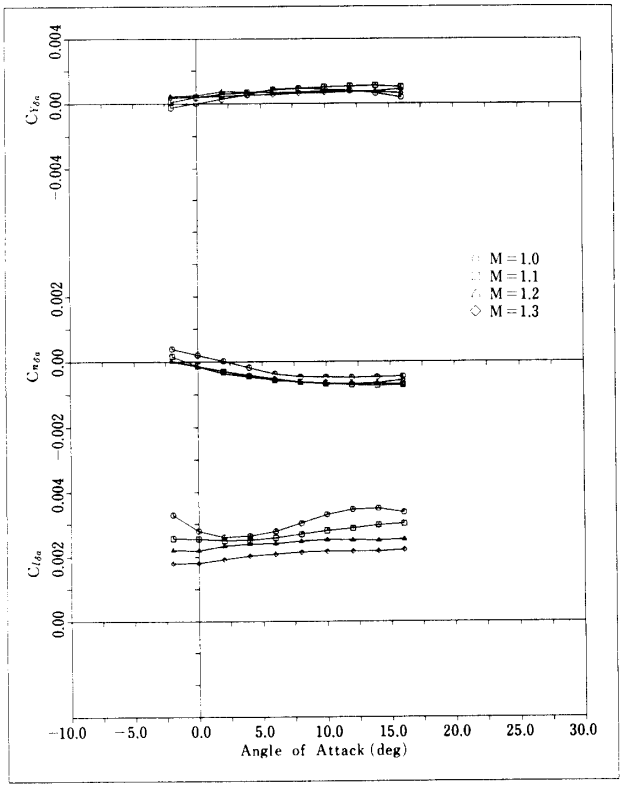

Fig. 9-b. Lateral directional aerodynamic derivatives of aileron deflection (M=1.0−1.3 based on δa=5 deg data).

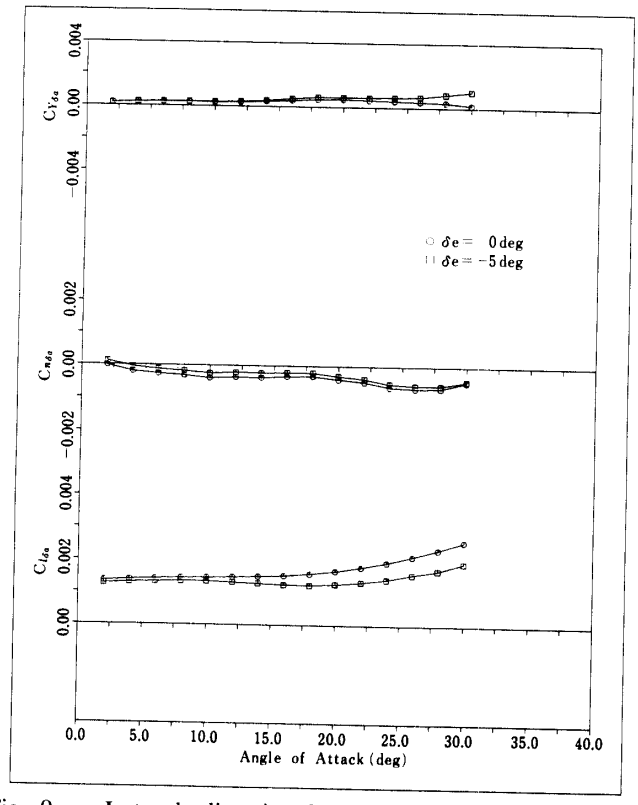

Fig. 9-c. Lateral directional aerodynamic derivatives of aileron deflection (M=1.6 based on δa=5 deg data).

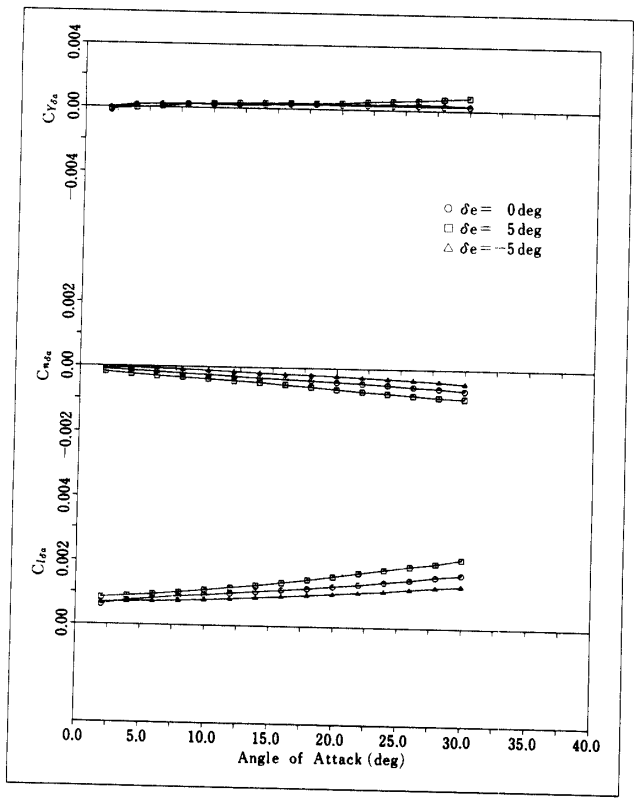

Fig. 9-d. Lateral directional aerodynamic derivatives of aileron deflection (M=2.5 based on δa=5 deg data).

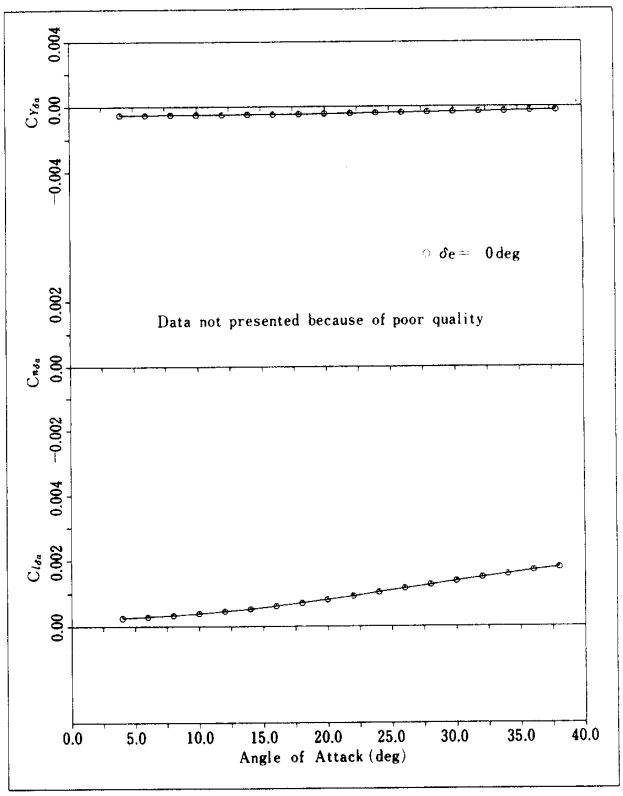

Fig. 9-e. Lateral directional aerodynamic derivatives of aileron deflection (M=7.0 based on δa=5 deg data).

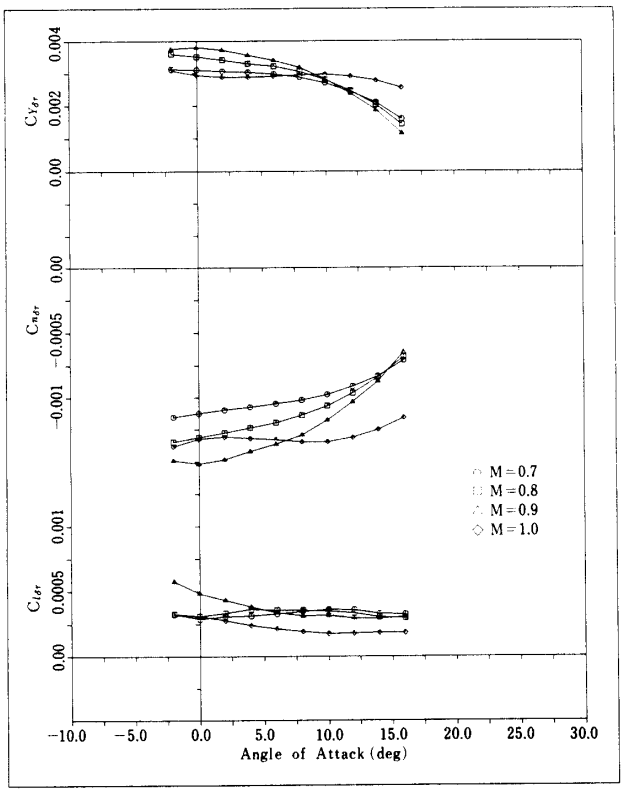

Fig. 10-a. Lateral directional aerodynamic derivatives of rudder deflection (M=0.7−1.0 based on δr=30 deg data).

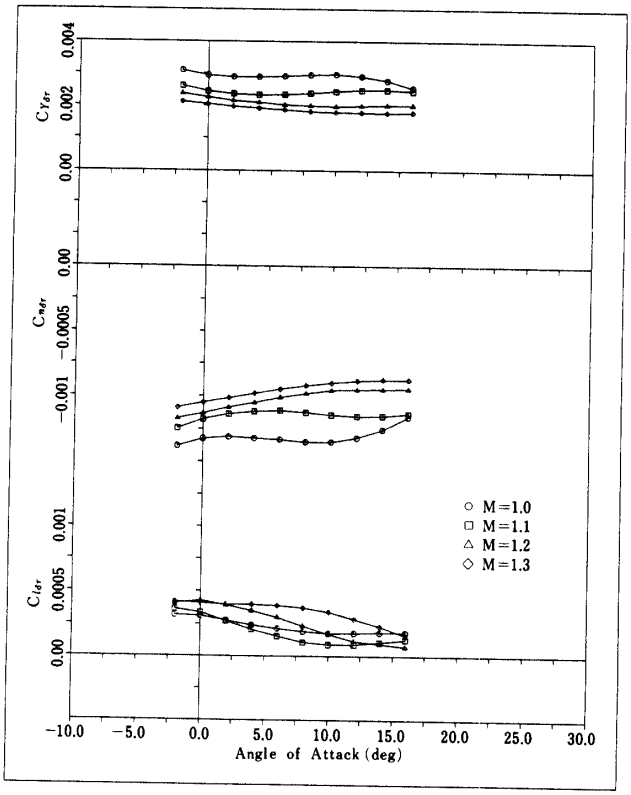

Fig. 10-b. Lateral directional aerodynamic derivatives of rudder deflection (M=1.0−1.3 based on δr=30 deg data).

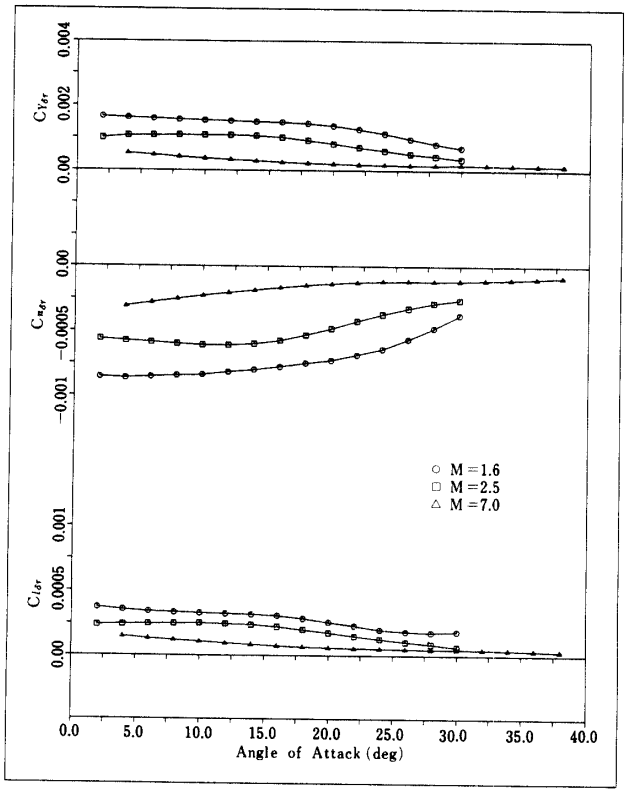

Fig. 10-c. Lateral directional aerodynamic derivatives of rudder deflection (M=1.6−7.0 based on δr=30 deg data).

results of both tail-on and off configurations in the entire Mach number range of the present experiment are included in Figs. 8–10, and the results of single and double tailed configurations in the supersonic and hypersonic regions are also presented for comparison of the tail effectiveness. Since the measured data for lateral/directional aerodynamic coefficients of the highest Mach number (M=7) are of poor quality because of the lack of repeatability, some of these results are not presented here.

Data accuracy of the measurement based on the repeatability and compensation of forces and moments, resulting from various reasons such as misalignment and the setting error of the model, gauge balance and/or the sting support in each testing, is estimated as

$$0.005 \text{ for } C_L,\ C_D \text{ and } C_Y$$
$$0.002 \text{ for } C_m$$
and $$0.001 \text{ for } C_l \text{ and } C_n$$

in terms of the magnitude of measured aerodynamic coefficients (not of processed aerodynamic derivatives). These values are for the worst condition which are at the lowest speed condition of transonic testing and at the hypersonic testing. Derivatives of elevon deflection and lateral/directional aerodynamic coefficients presented in the following results are obtained by the data that are nearly 5 degrees of side slip angle, 10 or 20 degrees of elevator deflection angle, 5 degrees of aileron deflection and 30 or 60 degrees of rudder or speed brake deflection respectively. These values are indicated in each figure.

4. Discussion

4–1. Longitudinal Aerodynamic Characteristics

As shown in Fig. 4, lift and drag characteristics are fairly similar to those of conventional aircraft from low to high Mach number regions. At the high angle of attack attitude condition, although the slight nonlinearity in these coefficients is observed in subsonic and higher Mach number region, no abrupt change in the longitudinal characteristics which appears in low speed region is observed in these ranges.

Pitching moment coefficient slope is negative, so that the vehicle is aerodynamically stable at subsonic to low supersonic range except for the angle of attack greater than 10 degrees in subsonic range. However, it must be remarked that the pitching moment slope is nearly zero or slightly positive; neutral to unstable at higher Mach number range. This characteristics is not favorable in terms of flight dynamics and further improvement on planform geometry must be made to refine the pitching moment characteristics.

Since the results for Mach number of 5 and 7 show no substantial difference in pitching moment curve, it can be regarded that these results present typical hypersonic characteristics and that the same characteristics will be observed in much higher Mach number regions.

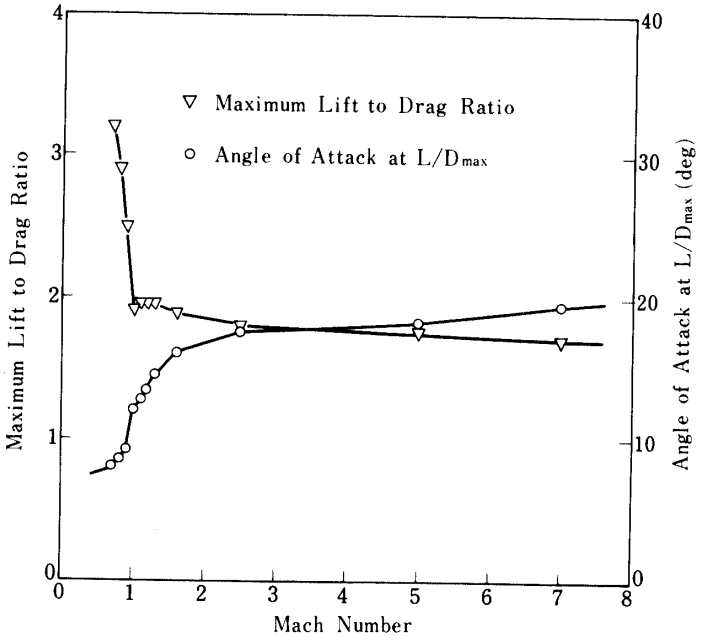

Fig. 11. Maximum L/D and angle of attack of L/D max

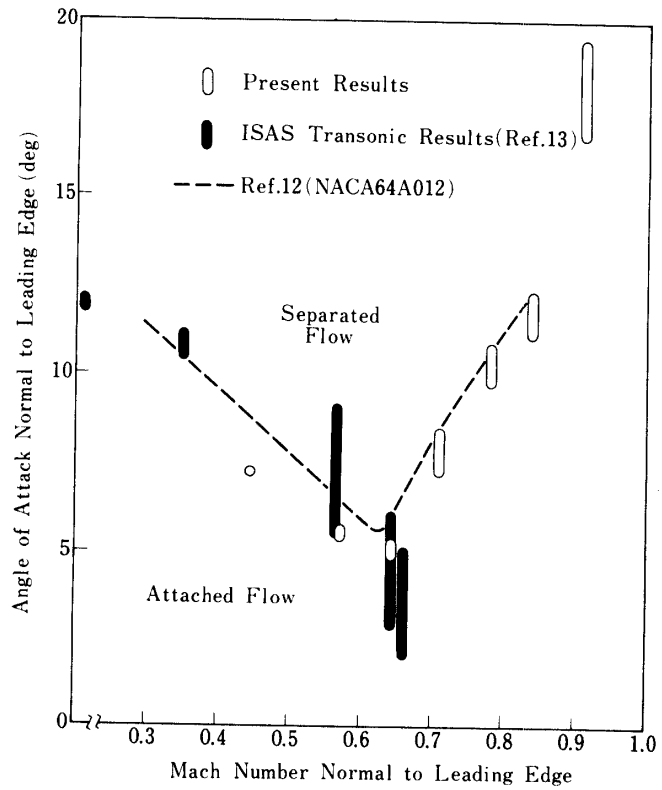

Fig. 12. Relation between speed and attitude at which wing leading edge separation takes place.

The effect of the elevator deflection on the pitching moment coefficient $Cm_{\delta e}$ is about 0.01 per degree in subsonic region. It becomes smaller as Mach number increases. In the higher Mach number region, $Cm_{\delta e}$ is about half to one third of that at subsonic range. Test result shows that it is greater as angle of attack increases in hypersonic region. This implies that the Newtonian impact analogy may be possible in predicting elevon deflection coefficient in these and much higher Mach number regions.

The maximum value of untrimmed lift to drag ratio (L/D) is presented in Fig. 11 where the angle of attack at which the maximum L/D is attained is also presented. As is seen in the figure, although the longitudinal trim at the angle of attack of about 10 degrees is desirable in subsonic region, it will not be achieved by use of the present elevator in subsonic to low supersonic region. Taking the fact into account that the nose-droop of the body produces nose-down moment, it is obvious that the reason for the high angle of attack trim capability at hypersonic region may be attributed to the body configuration as is seen in Fig. 4-i and j. Anyway, further improvement seems to be required for the balance of low and high speed trim characteristics. Furthermore, the values of maximum L/D itself at low speed region is still lower than the preferable one for the horizontal landing. However, this will be easily improved by modification of body fineness ratio and aspect ratio of the wing.

In the subsonic Mach number range, lift coefficient curve slope is getting smaller for the angle of attack greater than 10 degrees. The same trend can be observed in pitching moment coefficient at the corresponding Mach number region. This non-linear characteristics seems to be brought about by flow separation at the wing leading edge in transonic region, which is influenced by the wing sweep back angle or the Mach number normal to the wing leading edge *[14]*. Fig. 12 shows the summarized result based on the data shown in Fig. 7 in terms of the relation between Mach number and angles of attack normal to the wing leading edge at which separation takes place. This angle is defined as the one at which nonlineality in lift curve slope appears. The result shows a typical trend of leading edge separation of delta wing which occurs in transonic region. Comparisons of the longitudinal characteristics in Fig. 6 indicate a significant improvement by installing forward delta wing or so called double delta wing planform which has the forward part having greater sweep back angle than main wing. It must be noted that there is no remarkable difference between two types of double delta wing, so far as the longitudinal characteristics are concerned.

As is seen in Fig. 7-a and b, the present speed brake has sufficient effectiveness on control of vehicle's drag. Moreover, the speed brake affects the pitching moment enough so as to be used as a longitudinal trimming device. However, some difficulties may arise in the longitudinal trimming performance because the effectiveness of the speed brake presents unfavorable non-linear effect to the pitching moment characteristics in the speed range studied.

4–2. Lateral/Directional Aerodynamic Characteristics

Aerodynamic coefficients related to lateral/directional stability and controllability are influenced very much by both angle of attack and Mach number. This trend is

quite same as observed in the longitudinal aerodynamic characteristics. In the aerodynamic design of the present reentry vehicle, the effect of tail wing on the lateral/directional stability is of a great interest.

Stable dihedral effect in rolling moment coefficient slope is attained within the entire Mach number range, and as shown in the test results, it is clear that the rolling moment generated by the tail has a relatively large effect. On the other hand, yawing moment coefficient that determines the directional stability shows less stability than that for the conventional airplanes. Although it is positive in the range from subsonic to low supersonic speed, it becomes negative at high angles of attack in case the higher Mach number is approached. Furthermore, the directional stability turns out to be more unstable as the angle of attack increases because of the wake of the fore-body. The effect of tail wing on the directional stability diminishes as Mach number increases, whereas the unstable yawing moment generated by fore-body is not so influenced by Mach number, indicating that the directional instability may be unavoidable in much higher speed range. Of course, although extremely large size of the tail wing may overcome the foregoing difficulty, it does not seem to be of a practical solution.

In the range of low subsonic speeds, it is well known that the conventional aircraft have a trend to change abruptly the lateral directional stability characteristics as a certain angle of attack is approached, because the stall due to flow separation takes place on the main wing. This seemingly discontinuous change in lateral/directional characteristics affects so much the flight performances of the aircraft at high angle of attack. However, so far as the present result is concerned, no abrupt change is observed in both rolling and yawing moment coefficients at high angle of attack in high supersonic to hypersonic speed range.

Comparison of the lateral/directional derivatives at supersonic speed between double tail and single tail configurations (see Figures 8-d, e and f) leads to the conclusion that the single tail is advantageous in low supersonic region and that the double tail has slight advantage in directional stability in case the angle of attack is greater than 30 degrees. Thus, the tail modification seems to induce a considerable amount of the associated difference in dihedral effect, as shown in the figures. From view point of the flight dynamic characteristics, balance between the dihedral effect and the directional stability is an important design factor so that the tail configuration must be determined through a significant analysis on stability and controllability of the vehicle.

Aerodynamic derivatives of aileron deflection $Cl_{\delta a}$ indicates that it is large enough to control the rolling moment caused by side slip. It can be also observed in the present results that $Cl_{\delta a}$ increases as either the angle of attack or the deflection angle increases, as the results of $Cm_{\delta e}$. On the contrary, the induced yawing moment due to the aileron deflection $Cn_{\delta a}$ shows a rather complicated behavior, that is, it has a proverse yaw characteristics in subsonic region, whereas it has an adverse yaw characteristics in supersonic and hypersonic region. Furthermore, it is affected by both angle of attack and elevator position. Both the sign and the magnitude of $Cn_{\delta a}$ are the important aerodynamic factors for determining the lateral/directional

controllability especially at high angle of attack, where vehicle's directional stability becomes poor.

In the transonic region, yawing moment produced by rudder deflection $Cn_{\delta r}$ seems to be satisfactory for compensating the directional stability coefficient. However, the rudder becomes less effective as the angle of attack increases in the higher Mach number region, that is, the higher the angles of attack and the Mach numbers are, the worse the effectiveness is. The defect is clearly due to the body wake which reduces the dynamic pressure acting on the tail and the rudder surfaces. Notwithstanding that the rudder effectiveness is also one of the most important derivatives in flight control characteristics, the present series of wind tunnel testing did not provide sufficient data related to the rudder effectiveness for single tail configuration. Consequently, further investigation must be made from view point of the aerodynamic design of the tail configuration that essentially determines the lateral/directional flight dynamic characteristics.

5. Concluding Remarks

Static aerodynamic coefficients of a winged space vehecle recently developed in ISAS have been investigated from view point of the longitudinal and lateral/directional stability and controllability through a series of wind tunnel testing. All coefficients and their derivatives, obtained as the function of angle of attack and Mach number, have been examined in detail in conjunction with the vehicle's configuration, and the results may be summarized as follows;

1. Maximum Lift to drag ratio at low subsonic speed is rather smaller than that will be required for the safety landing to a run way.
2. Balances in longitudinal stability between low and high speed region must be improved if aerodynamically stable flight dynamic performance is directed.
3. The low speed longitudinal trim capability by elevator deflection is insufficient if the present center of gravity position is selected to achieve a high angle of attack trim at hypersonic speed regions.
4. Double delta wing planform having a higher sweep back angle than the main wing improves transonic longitudinal stability at large angles of attack.
5. In the case of present size of tail wing, the directional stability derivative at high angles of attack becomes negative as Mach number increases.
6. The single tail configuration is favorable for directional stability at low supersonic region, whereas the double tail is of advantage at high angle of attack in the higher speed region.
7. At high angles of attack and high flight speeds, the rudder effectiveness seems to be poor to compensate the unstable yawing moment due to side slip.

The fifth and the last statements in the conclusion above seem to be an inherently given and unavoidable in designing such a winged reentry vehicle, whereas the remaining ones; 1, 2 and 3 etc, will be able to be improved by the modification of

vehicle's configuration. Any way, these must be concluded after the sufficient investigation on flight dynamics or the closed-loop control analysis of the vehicle along the trajectory or the history of Mach number and angle of attack of the recentry flight.

Acknowledgement

The authors express their sincere thanks to the personnel of transonic, supersonic and hypersonic wind tunnels of National Aerospace Laboratory for their cooperation in executing the wind tunnel testing and measurement. The authors also express their gratitude to Prof. H. Oguchi who is the director of the Working Group for Winged Space Vehicle of ISAS and has given the opportunities to the authors to carry out the present series of wind tunnel testing.

References

[*1*] Freeman, D. C., Jr. and Powell, R. W. "The Results of Studies to Determine the Impact of Far-Aft Center-of-Gravity Locations on the Design of Single Stage to Orbit Vehicle System", J. Spacecraft and Rocket, Vol. 17, No. 4, 1980

[*2*] Wawrztniak, M. E. "To What extent Should Space Shuttle Stability and Control be Provided through Stability Augumentation", NASA Washington Space Transportation System Technology Symposium, Vol. 1, July, 1970

[*3*] Hepler, A. K., Zeck, H., Walker W. H. and Polak, A., "A Study of Flight Control Requirements for Advanced, Winged, Earht-to-Orbit Vehicles With Far-Aft Center-of-Gravity Locations", NASA CR-3491, 1982

[*4*] Hepler, A. K., Zeck, H., Walker, W. H. and Shafer, D. E., "Applicability of the Control Configured Design Approach to Advanced Earth Orbital Transportation Systems", NASA CR-2723, 1978

[*5*] Bennett, D. E. "Space Shuttle Entry Flight Control Overview", J Astronautical Sciences, vol. XXXI, No. 4, 1983, pp 569–578

[*6*] Gamble, J. D. "The Application of Aerodynamic Uncertainties in the Design of the Entry Trajectory and Flight Control System of Space Shuttle Orbiter, Shuttle Performances: Lessons Learned", NASA CP-2283, 1983, pp 595–616

[*7*] Whitnah, A. M. and Hillje, E. R., "Space Shuttle Wind Tunnel Testing Program Summary", NASA TP 1125, 1984

[*8*] Boyden, R. P. and Freeman, D. C., Jr., "Subsonic and Transonic Stability Characteristics of A Space Shuttle Orbiter", NASA TN D-8042, 1975

[*9*] Freeman, D. C. Jr. and Boyden, R. P., "Supersonic Stability Characteristics of A Space Shuttle Orbiter", NASA TN D-8043, 1975

[*10*] Nagatomo, M., Naruo, Y. and Inatani, Y., "A Concopt of Highly Maneuverable Experimental Space (HIMES) Vehicle", IAF 85–137, 1985

[*11*] 航空技術研究所 "航空技術研究所 2 m × 2 m遷音速風洞の計画と構造", 航空技術研究所報告 NAL TR-25, 1962

[*12*] 空気力学第2部 "1 m × 1 m吹出式超音速風洞の計画と構造", 航空技術研究所報告 NAL TR-29, 1962

[*13*] 極超音速風洞建設グループ, "50cm極超音速風洞の計画と構造", 航空宇宙技術研究所報告 NAL TR-116, 1966

[*14*] Stanbrook, A. and Squire, L. C., "Possible Types of Flow at Swept Leading Edges", The Aeronautical Quarterly, Feb. 1964, pp 72–82

[*15*] Inatani, Y. "Aerodynamic Characteristics of Winged Space Vehicle", ISAS Working Group for Winged Space Vehicle Internal Report, 1984